INVITED FEATURE PAPER

Review

The evolution of low temperature solid oxide fuel cells

Kang Taek Lee, Hee Sung Yoon, and Eric D. Wachsman[a)]
University of Maryland Energy Research Center, University of Maryland, College Park, Maryland 20742

(Received 21 February 2012; accepted 16 May 2012)

Low temperature solid oxide fuel cells (SOFCs) are a promising solution to revolutionize stationary, transportation, and personal power energy conversion efficiency. Through investigation of fundamental conduction mechanisms, we have developed the highest conductivity solid electrolyte, stabilized bismuth oxide ($Dy_{0.08}W_{0.04}Bi_{0.88}O_{0.36}$). To overcome its inherent thermodynamic instability in the anode environment, we invented a functionally graded bismuth oxide/ceria bilayered electrolyte. For compatibility with this bilayared electrolyte, we developed high performance bismuth ruthenate–bismuth oxide composite cathodes. Finally, these components were integrated into an anode-supported cell with an anode functional layer, resulting in an exceptionally high power density of ~2 W/cm^2 at moderate temperatures (650 °C) and sufficient power down to 300–400 °C for most applications. Moreover, because SOFCs can operate on conventional fuels, these low temperature SOFCs provide one of the most efficient energy conversion technologies available without relying on a hydrogen infrastructure.

I. INTRODUCTION

Transforming automotive power sources into higher efficiency technologies is vital to the stability of our environment, energy supply, and economy. The urgency of this transformation resulted in a major focus on plug-in hybrid electric vehicles (PHEVs). However, if the PHEVs are charged by conventional coal power plants at night and conventional internal combustion (IC) engines while in transit, the "well to wheels" reduction in CO_2 is limited to the increase in efficiency gains afforded by the electric drive hybrid technology, rather than an increase in the actual hydrocarbon to electricity energy conversion process.

Moreover, the range and cost of PHEVs are limited by the energy density of the batteries; and no current battery can compare on a kWh/kg or kWh/L basis with a liquid-fueled energy conversion (hydrocarbon to electricity) process. Unfortunately, IC engines are limited by Carnot efficiency, are far from pollution free, and convert chemical energy to mechanical energy rather than electric power needed by an electric drive vehicle thus requiring an additional mechanical to electrical energy conversion step. In contrast, the use of fuel cells (FCs) rather than an IC engine in a PHEV would result in a dramatic improvement in efficiency, reduction in emissions, and is directly amenable to an electric drive system.

For high efficiency energy conversion, there has been a tremendous effort to develop solid oxide fuel cells (SOFC) operating at temperatures below 900 °C for cost and reliability considerations. Simultaneously, there has been an even larger effort to increase the operating temperature of proton exchange membrane fuel cells (PEMFC) above 100 °C for performance and fuel poisoning considerations. Somewhere in between is the optimum operating temperature for a FC depending on fuel choice and degree of external fuel processing (versus relying exclusively on internal reforming). While there has been some success at developing high temperature PEMFCs operating at temperatures around 140 °C, the power densities and fuel flexibility of these systems are limited. Moreover, there is significant concern that the hydrogen infrastructure necessary for PEMFCs will always make this a future technology with limited market penetration. In contrast, SOFCs can operate on both current conventional fuels (e.g., natural gas, gasoline, and diesel) and biofuels (e.g., biogas, ethanol, and biodiesel). As such, SOFCs offer great promise as a clean and efficient process for directly converting chemical energy to electricity while providing significant environmental benefits. SOFCs produce negligible CO, HC, or NO_x and, as a result of their high efficiency, produce about one-third less CO_2 per kWh than IC engines. Moreover, SOFC operation on biofuels is the most energy efficient means to utilize home grown carbon neutral fuels.

Therefore, SOFCs are the most efficient technology for converting energy from hydrocarbon fuels to electricity on a "well to wheels" basis. On a system basis, SOFCs hold the potential for producing the least CO_2/kWh from conventional fuels. If designed to operate on a renewable resources like biofuel, SOFCs would effectively be carbon neutral. Such a vehicle development would be a transformational change in transportation technology. Not only could low temperature, SOFCs transform the automotive sector as a range extender for PHEVs, but this enabling

[a)]Address all correspondence to this author.
e-mail: ewach@umd.edu
This paper has been selected as an Invited Feature Paper.
DOI: 10.1557/jmr.2012.194

 © Materials Research Society 2012

https://doi.org/10.1557/jmr.2012.194 Published online by Cambridge University Press

technology would impact numerous other industries from personal power to large-scale power production.

As an auxiliary power unit, this technology could transform the energy efficiency and emissions of the rest of the transportation sector (trucks, boats, trains, and airplanes), which have to operate large engines in their most inefficient mode (idle) to maintain electric power. SOFCs are modular and can be made in sizes ranging from mW to MW. By driving down the temperature, the door opens to a whole host of small personal power applications from battery replacements (mW to W) to battery chargers (~100 W) for both civilian and military applications. Operating on natural gas, SOFCs could provide more efficient combined heat (including hot water) and power units for residential (~10 kW) and commercial (~200 kW) use.[1,2]

Unfortunately, current SOFC technology must operate in the temperature region of ~800 °C to avoid unacceptably high ohmic losses with conventional zirconia-based electrolytes. These high temperatures demand specialized and expensive materials for the FC interconnects and insulation and significant time and energy to heat up to the operating temperature. Therefore, development of SOFCs to provide reasonable power output at lower temperatures (≤600 °C) would make SOFCs both more cost competitive with conventional technology and significantly reduce start-up times, which are critical to transportation and portable power applications.[1,3]

To address the issue mentioned above, alternative oxide electrolytes with higher conductivities have been considered to allow operation at lower temperatures. Materials considered range from gallates and ceria to bismuth oxide-based materials. However, each of these materials has their own specific issues. Moreover, transitioning from a zirconia electrolyte to one of these alternate electrolytes requires development of an entirely new cell material set.

Over the last 20 years, we have focused on using the most conductive, and hence lowest temperature, bismuth oxide-based electrolyte.[4–17] To overcome its inherent instability in reducing environments, we developed a bilayer bismuth oxide/ceria electrolyte.[18] To avoid reactivity of bismuth oxide with more conventional cathode materials, we developed a bismuth ruthenate/bismuth oxide composite cathode.[19,20] Finally, these materials were integrated into an anode-supported cell resulting in power densities of ~2 W/cm^2 at 650 °C.[21,22] These SOFCs demonstrate sufficient power down to 400 °C, thus attaining the temperature "sweet spot" necessary to transform FC technology. In this paper, we review effort over the last 20 years to develop high performance lower temperature SOFCs.

II. DEVELOPMENT OF HIGH PERFORMANCE ELECTROLYTES FOR LT-SOFCs

A. Higher conductivity electrolytes

For lower SOFC operation temperature, the ohmic polarization resistance should be suppressed due to its thermally activated nature.[23] One of the most successful approaches for lowering the resistance of a solid electrolyte is ultrathin electrolyte design (<~15 μm).[24] With this approach, it was shown that yttria-stabilized zirconia (YSZ), a conventional electrolyte for high temperature SOFCs, can have a reasonably low area-specific resistance (ASR) (~0.15 Ωcm^2) at around 700 °C.[25] However, below that temperature, it must be ~1-μm thick to achieve the same ASR, and this introduces processing issues. Alternatively, higher ion conductivity electrolytes have been studied and applied. Among these materials, our research has focused on isovalent cation-doped stabilized bismuth oxide and aliovalent cation-doped ceria.

1. Stabilized bismuth oxide

Phase-stabilized bismuth oxide electrolytes have been known to have the highest oxygen conductivity among the studied electrolytes.[26] Various polymorphs in bismuth oxides have been identified, with α, β, γ, and δ phases.[27] Even though the cubic δ phase with fluorite structure at high temperature (>729 °C) shows an excellent ionic conductivity, attributed to the presence of such a large concentration (25%) of oxygen vacancies, it is unstable and transforms into a monoclinic phase below 729 °C resulting in a discontinuous decrease in conductivity.[28] However, when a solid solution of bismuth oxide is formed with various rare earth oxides, it maintains the high temperature defective fluorite structure down to room temperature. This results in high conductivity at much lower temperature, thus making it a promising electrolyte for low temperature (LT) SOFC.[29] Based on literature, ASRs of YSZ, gadolinia doped ceria (GDC), and erbia-stabilized bismuth oxide (ESB) with thickness of 10 μm are 1.259, 0.145, and 0.037 Ωcm^2, respectively, at 500 °C (Fig. 1).[15] These data indicate that when using stabilized bismuth oxide, the ohmic polarization can be reduced by 1–2 orders of magnitude without compromising electrolyte thickness.

For the last two decades, we have intensively studied the effect of oxygen sublattice structure and ionic transport on conductivity in these highly defective fluorite oxides.[4–11,14] The structure of fluorite bismuth oxide is a combination of a fcc cation sublattice and oxygen ions in six of the eight tetrahedral sites. Moreover, in contrast to aliovalent cation-doped ceria or zirconia, bismuth oxides stabilized by isovalent cations have no electrostatic difference between host (Bi^{3+}) and dopant, while maintaining a high fraction of oxygen vacancies with 25% of the anion sites. Thus, this high ionic conduction strongly depends on the arrangement of the two oxygen vacancies in the anion sublattice in a unit cell without consideration of Coulombic attraction.[14] Based on previously proposed structural models for δ-Bi_2O_3,[30–32] we determined that the fluorite structure of bismuth oxide consists of a disordered oxygen sublattice with a short-range ordering of oxygen

https://doi.org/10.1557/jmr.2012.194 Published online by Cambridge University Press

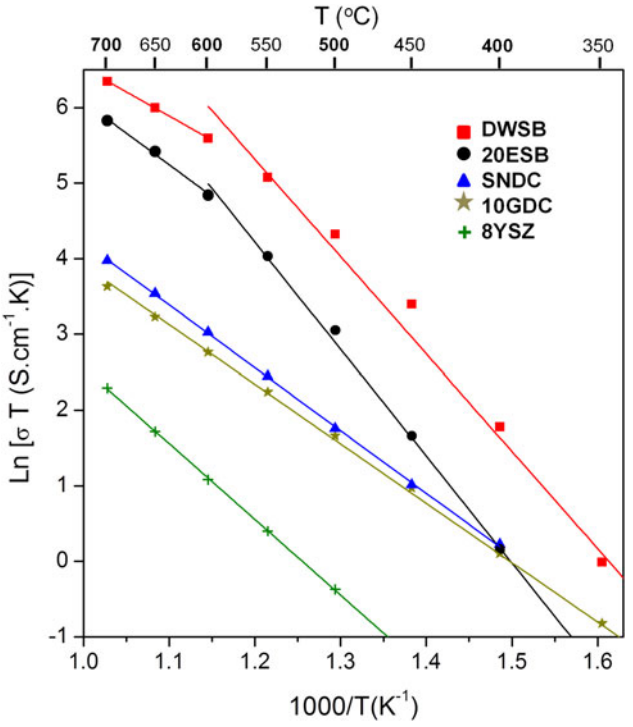


FIG. 1. Comparison of conductivity of various solid electrolytes.[1] (8YSZ—$Y_{0.16}Zr_{0.92}O_{2.08}$, 10GDC—$Gd_{0.1}Ce_{0.9}O_{1.95}$, SNDC—$Sm_{0.075}Nd_{0.075}Ce_{0.85}O_{2-\delta}$, 20ESB—$Er_{0.4}Bi_{1.6}O_3$, DWSB—$Dy_{0.08}W_{0.04}Bi_{0.88}O_{1.56}$.)

vacancies along the <111> directions.[9,10] In addition, from our neutron diffraction studies, we have experimentally confirmed extensive displacement of oxygen ions from regular 8*c* sites to interstitial 32*f* sites.[10,11] In this structure, the ionic transport mechanism is more complicated than simple hopping between the regular tetrahedral sites along the <100> directions due to the presence of vacant octahedral sites. Thus, there are more energetically favorable paths involving the displacement of oxygen ions toward the central vacant position along the <111> directions (Fig. 2) resulting in a local structural dependence on ionic conductivity.[10]

For most of the bismuth oxides stabilized with lanthanide dopants (Dy, Ho, Er, Tm, and Yb), the conductivity activation energy (E_A) increases below 600 °C due to an order–disorder transition of the oxygen sublattice.[8] Moreover, at this temperature (<600 °C), the stabilized bismuth oxides experience time-dependent conductivity degradation. Our results revealed that this conductivity decay of lanthanide-doped Bi_2O_3 is not due to phase transformation, which is a main reason for conductivity degradation of some doped Bi_2O_3 at higher temperature (>600 °C), but due to anion ordering within the cubic fluorite structure–stability window. Transmission electron microscopy (TEM) observations showed a superstructure with the alignment of vacant 8*c* anion sites in <111> direction, indicating occupational ordering.[9] In addition, analysis of neutron diffraction patterns indicated positional ordering, which can be explained by displacement of the occupied anion sites in a <111> direction from 8*c* to 32*f* sites. In a modeling study based on these TEM and neutron diffraction studies, we concluded that this aging phenomenon is the result of combination of occupational ordering and positional ordering.[9,10,14]

Further studies of the effect of dopant radii and concentration have shown that the ionic radii and polarizability of dopant cations influence the kinetics of vacancy ordering in the oxygen sublattice, thus affecting stability of conductivity below the order–disorder transition temperature.[12] These results showed that most lanthanide dopants used to stabilize the fluorite Bi_2O_3 are less polarizable than host cation (Bi^{3+}) and the stability of the disordered oxygen sublattice was improved as dopant radii and polarizability increased. Thus, the highest stability for the disordered anion sublattice was obtained with Dy, which has both large ionic radii and high polarizability.[8,12] Moreover, simulation results revealed that polarizability is more important than radii for determining oxygen diffusion in Bi_2O_3, leading to a disordered lattice.[33,34] Other studies pointed out W as a highly attractive dopant to stabilize the cubic Bi_2O_3 structure due to its high polarizability.[35,36] Accordingly, we developed a stabilized bismuth oxide with double dopants, Dy and W (DWSB).[13] Using the double dopant strategy, bismuth oxide was stabilized with less total dopant concentration, only ~12 mol%. Finally, we achieved a conductivity of 0.57 and 0.098 S/cm at 700 and 500 °C, respectively, with a composition of $(DyO_{1.5})_{0.08}(WO_3)_{0.04}(BiO_{1.5})_{0.88}$ (8D4WSB).[15–17] Comparing at 500 °C, the conductivity of DWSB is ~4×, 10×, and 100× higher than those of ESB, GDC, and YSZ, respectively (Fig. 1). Thus, this novel electrolyte (DWSB) creates great opportunity for high power density LT-SOFCs.

Despite the high conductivity of stabilized bismuth oxide electrolytes, they have not been used in solid electrochemical devices such as SOFCs due to their thermodynamic instability. Takahashi et al.[37] indicated that the critical Po_2 value below which stabilized bismuth oxide would decompose is the equilibrium oxygen pressure of a Bi/Bi_2O_3 mixture. The decomposition process may be simplified as:

$$Bi_2O_3 = 2Bi(s) + \frac{3}{2}O_2(g) \quad . \qquad (1)$$

The open circuit potential (OCP) from galvanic cells with an air cathode and metal/metal oxide anode was stable in oxygen partial pressures above $10^{-13.1}$ atm at 600 °C. This result showed that there was no contribution of electronic conduction to the total conductivity above the equilibrium oxygen potential of Bi/Bi_2O_3 mixture. Therefore, they concluded that the minimum oxygen partial pressure at 600 °C is $10^{-13.1}$ atm. On the other hand, Wang and other researchers[38,39] reported that the ionic conductivity of Bi_2O_3 could be measured without critical decomposition of Bi/Bi_2O_3 under an H_2/H_2O atmosphere. Later, we

https://doi.org/10.1557/jmr.2012.194 Published online by Cambridge University Press

reported that the measured conductivity of ESB was independent of Po_2 over the range 1–10^{-22} atm under O_2/Ar atmosphere, while, as shown in Fig. 3, ESB decomposed at low Po_2 (10^{-21} atm) with H_2 as confirmed by x-ray diffraction (XRD).[6] Thus, the stability of ESB in the Ar/O_2 atmosphere is probably due to slow heterogeneous kinetics in the absence of an active reducing agent, such as H_2. Therefore, to use bismuth oxide as a SOFC electrolyte, exposure to the reducing environment of the fuel gases must be prevented to limit decomposition.

2. Aliovalent cation-doped ceria

Aliovalent cation-doped ceria (CeO_2) has received attention as a potential solid electrolyte because it exhibits higher ionic conductivity than YSZ over a range of high to intermediate temperatures. The ionic conductivity of ceria is considerably increased by aliovalent cation doping, which increases the oxygen vacancy concentration.[40,41] The magnitude of electrical conductivity and the stability under reducing conditions for ceria-based oxides depend greatly on the kind and quantity of doping elements. Alkaline earth oxides (e.g., CaO and SrO) and rare earth oxides (e.g., Gd_2O_3 and Sm_2O_3) are highly soluble in the ceria sublattice. Among these, Sm^{3+}- and Gd^{3+}-doped ceria, which are close in ionic radii to Ce^{4+}, show the highest electrical conductivity in ceria-based oxides with 10–20% dopant concentration.[41] Moreover, Steele[42] claimed that the ionic conductivity of $Gd_{0.1}Ce_{0.9}O_{1.95}$ (10GDC) is the highest among various Gd and Sm dopant concentrations at a temperature range of 500–700 °C. Thus, 10GDC has gained attention as one of the most suitable candidates for SOFCs electrolytes at lower temperature ranges. At temperature below 800 °C, the ionic conductivity of doped ceria is approximately one to two orders of magnitude greater than that of stabilized zirconia, which is currently the most widely used electrolyte material. This is due in part because the Ce^{4+} (0.87 Å) ion has a larger ionic radius than Zr^{4+} (0.72 Å) resulting in easier oxygen ion migration through a more open structure.

In recent studies, we demonstrated even higher ionic conductivity for doped ceria at lower temperature using a codoping strategy.[43–45] Previous computational studies using density functional theory by Andersson et al.[46] predicted that, when Pm (atomic number 61) is selected as the dopant in ceria, the total interaction energy between

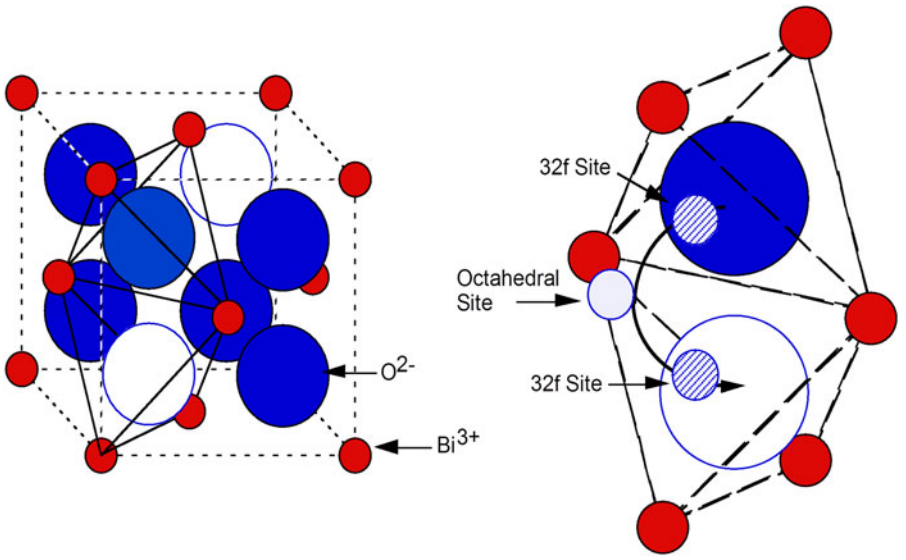


FIG. 2. Ionic transport mechanism in δ-Bi_2O_3 from one tetrahedron to an adjacent empty tetrahedron in <100> direction.[10]

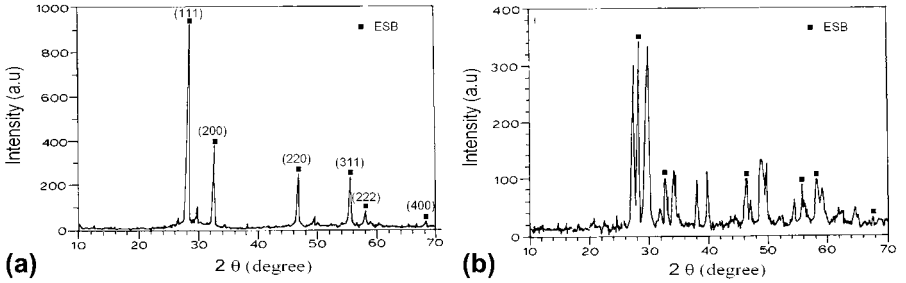


FIG. 3. X-ray diffraction of 20 mol% ESB: (a) as received; (b) annealed 4 h at 700 °C in H_2/H_2O $P_{O2} = 10^{-21}$ atm.[6]

https://doi.org/10.1557/jmr.2012.194 Published online by Cambridge University Press

oxygen vacancy and dopant cations is minimized rather than using other dopants such as Gd or Sm, thus maximizing oxygen ion conductivity. However, Pm is a radioactive element and an unrealistic selection for a SOFC electrolyte component. Therefore, to produce the effective atomic number of Pm^{3+} with ionic radius of 1.093 Å,[47] a codoping strategy was used based on our previous work of doubly doped bismuth oxides (DWSBs).[13] In this work, we chose a double dopant system with Sm^{3+} and Nd^{3+}, expecting average dopant ionic radius of 1.094 Å in 1:1 mixing ratio. Through a systematic study for composition and temperature dependence on grain ionic conductivity of these materials, the optimum composition obtained was at $Sm_{0.075}Nd_{0.075}Ce_{0.85}O_{2-\delta}$ (SNDC).[45] This codoped ceria electrolyte enhanced the grain ionic conductivity by 30% compared to that of 10GDC at 550 °C. Using this novel electrolyte, we recently demonstrated high power densities at lower temperature (500–650 °C) indicating SNDC as a promising electrolyte for LT-SOFC.[48]

However, ceria-based electrolytes also have a stability issue. When ceria-based oxides are reduced at low oxygen partial pressures ($<10^{-14}$ atm), Ce^{4+} transfers into Ce^{3+} leading to significant n-type electronic conduction with a $P(O_2)^{-1/4}$ dependence.[42] This mixed ionic and electronic conduction (MIEC) property of doped ceria electrolytes reduces the ionic transference number (t_i) and the OCP, thereby making ceria less efficient for application as a SOFC electrolyte.

In fact, it is easy to find inconsistency in OCPs reported by different research groups using doped ceria electrolytes.[3,49–51] This is caused not only by electrolyte quality but also by electronic leakage current through MIEC electrolytes.[3,50,52,53] To explain the behavior of MIEC electrolytes in actual SOFC operation conditions, we developed a continuum-level electrochemical model of mixed conducting materials.[49] The modeling results predicted the OCP dependence of SOFCs as a function of MIEC electrolyte thickness. Recent experimental results confirmed the model predictions that OCP decreases proportionally with electrolyte thickness due to increased leakage current, i.e., higher oxygen permeation flux [Fig. 4(a)].[54] Therefore, as shown in Fig. 4(b), the maximum power density (MPD) of a SOFC with MIEC electrolyte is produced at a certain optimal thickness as a result of the trade-off between decreasing OCP and reduced ohmic resistance with decreasing thickness. In contrast, for a pure ionic conductor such as a stabilized zirconia, thinner electrolytes produce higher performance due to lower ohmic polarization. This result indicates that different design strategies are required for SOFCs with MIEC electrolytes. On the other hand, increasing the electrolytic domain and preserving the ionic conductivity of the doped ceria by any means is important.

B. Ceria/bismuth oxide bilayered electrolyte

To overcome the inherent thermodynamic stability limitations of these two highly conductive oxides (stabilized bismuth oxide and doped ceria), we proposed a functionally graded bilayer electrolyte consisting of a layer of stabilized bismuth oxide on the oxidizing side and a layer of doped ceria on the reducing side.[18] In this arrangement, as shown in Fig. 5, the interfacial Po_2 between the two electrolytes can be controlled by the thickness ratio of the constituent layers. Therefore, a sufficiently thick ceria layer would protect the bismuth oxide layer from decomposing, by shielding it from very low Po_2, and the bismuth oxide layer would serve to block electronic flux inherent in MIEC ceria electrolytes. As a result, higher OCP can be obtained in the bilayered ceria/bismuth oxide electrolytes since a bismuth oxide electrolyte has been reported to have essentially pure ionic conduction down to $Po_2 = 10^{-20}$ atm.

In early cell tests, a SOFC with an ESB/Sm-doped ceria (SDC) bilayered electrolyte using Pt and Au electrodes produced 35% greater power density than one with a SDC single electrolyte layer [Fig. 6(a)]. Moreover, the OCP of bismuth oxide/ceria bilayered electrolytes was stable up to 1400 h under open circuit and MPD condition [Fig. 6(b)]. The OCP and t_i of ESB/SDC bilayered electrolytes in an electrolyte-supported SOFC configuration were further investigated as a function of thickness ratio and

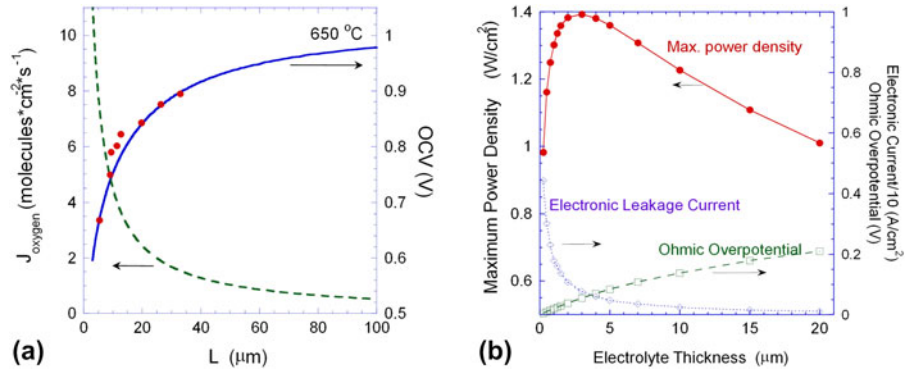


FIG. 4. (a) Open circuit voltage (OCV) and oxygen permeation flux as a function of electrolyte thickness at 650 °C. (b) Projected MPD, electronic (leakage) current, and ohmic overpotential as a function of electrolyte thickness predicted from model at 600 °C for Ni–SDC/SDC/BSCF.[54]

https://doi.org/10.1557/jmr.2012.194 Published online by Cambridge University Press

operation temperature with H_2/H_2O on the anode side and air on the cathode side.[55] As shown in Fig. 7, the OCP and t_i of the bilayered electrolyte improved with increasing relative ESB/SDC thickness, due to greater electronic blocking effect, and decreasing temperature due to the extended ionic domain of the ceria electrolyte. The measured OCP at 500 °C was 1006 mV approaching near the theoretical value. However, in this early study, we tested only low relative thickness ratio ($<\sim 0.03$) and used Au electrodes with poor electrocatalytic reactivity. Thus, a greater relative ESB thickness and better cathode should result in even greater OCP and t_i.

In addition to the effect of the bilayered electrolyte on OCP, the electrolyte ASR can be effectively reduced using this functionally graded electrolyte.[56] For example, the total ohmic ASR of the ESB/GDC bilayered electrolyte can be estimated by a simple two series resistor model:

$$\mathrm{ASR}_{\mathrm{electrolyte}} = L_{\mathrm{GDC}}\left(\frac{\tau}{\sigma_{\mathrm{ESB}}} + \frac{1}{\sigma_{\mathrm{GDC}}}\right) \quad , \qquad (2)$$

where L_{GDC} is thickness of GDC electrolyte, τ is thickness ratio of ESB to GDC, and σ_{ESB} and σ_{GDC} are the conductivities of ESB and GDC, respectively.[21] Figure 8 shows the calculated ASR for three ceria-based bilayered electrolytes at 500 °C with total thickness of 10 μm as a function of relative thickness. The ohmic ASR decreases dramatically with increasing relative thickness of the higher conductivity bismuth oxide layer. Moreover, actual measurements showed the effective conductance of ESB/SDC (20-μm/1.27-cm thick) was slightly higher than that of a 1.27-cm-thick SDC electrolyte. This result is due to the formation of a solid solution of bismuth/bismuth oxide in the ceria grain boundaries, forming paths with lower activation energy for oxygen ion transfer due to a scavenging effect on impurity phases.[57]

Figure 8 also shows that significantly lower electrolyte ASR's are achievable with a bilayer of our recently discovered DWSB and SNDC electrolytes. Further discussion of this can be found in our previous publication.[1] Moreover, it demonstrates the problem with using YSZ blocking layers as proposed by others[58,59] in that even ~1-μm YSZ layer essentially doubles the ASR relative to GDC alone.

While these early results demonstrate bilayered electrolytes improve the power density and OCP, the initial MPD measured was only ~53 mW/cm^2 at 800 °C due to use of low electrocatalytic activity cathodes (Au) and high ohmic resistance from the thick (~800 μm) electrolyte (Fig. 6).[18]

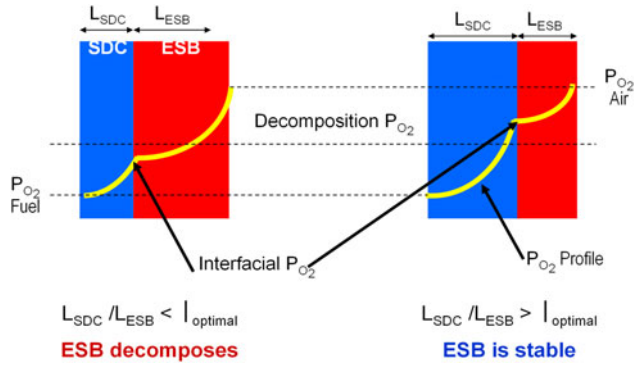


FIG. 5. Schematic diagram of ceria/bismuth oxide bilayered electrolyte concept.[18]

III. DEVELOPMENT OF HIGH PERFORMANCE CATHODES FOR LT-SOFCs

A. Investigation into fundamental cathode mechanisms

Cathodic polarization is a major roadblock to achieving SOFC operation at lower temperatures. It is well known that the greatest portion of activation polarization originates from sluggish kinetics of the oxygen reduction

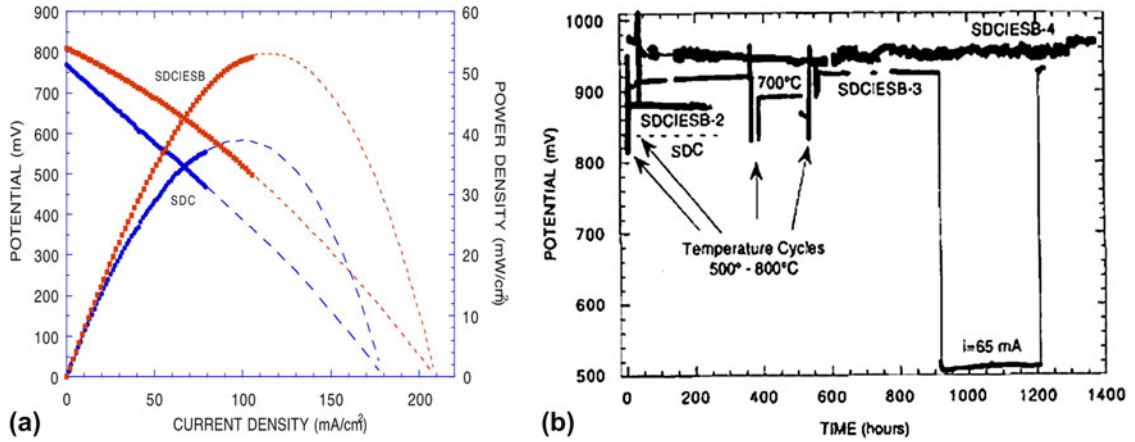


FIG. 6. (a) Comparison of cell performance of SDC/ESB electrolytes; ~1 mm electrolyte, Pt–H_2/H_2O anode, Au–O_2 cathode, 800 °C. (b) Stability of bilayered SDC/ESB electrolytes, as demonstrated by open circuit and maximum power potentials as a function of time. All data taken at 650 °C except where indicated. Breaks in the curve indicated I–V data acquisition.[18]

https://doi.org/10.1557/jmr.2012.194 Published online by Cambridge University Press

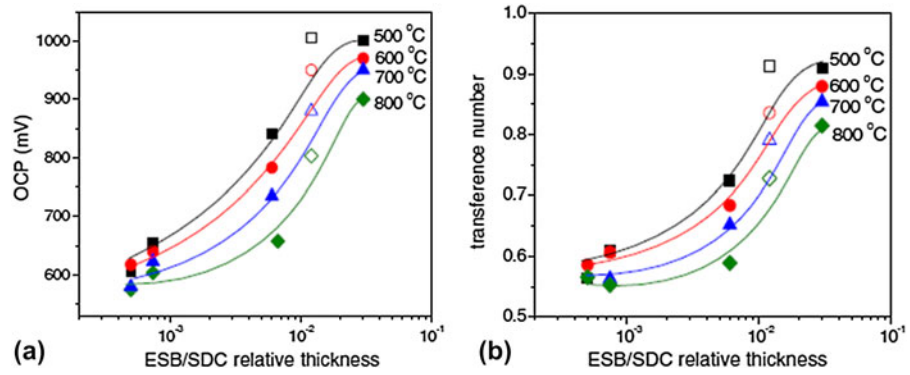


FIG. 7. Effect of ESB/SDC relative thickness and cathode on (a) OCP and (b) t_i (transference number) relation of bilayer electrolyte SOFC with air on the cathode side and H_2/H_2O on the anode side (open symbol Ag–ESB cathode and closed symbol Au cathode).[55]

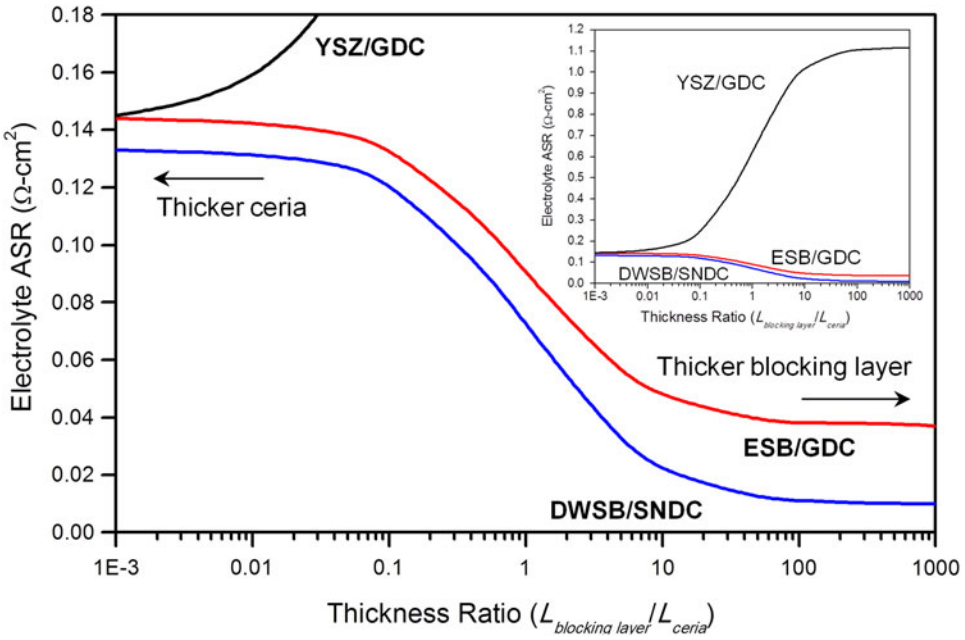


FIG. 8. Bulk electrolyte ASR at 500 °C as a function of relative ($\tau = L_{\text{blocking layer}}/L_{\text{ceria}}$) for YSZ/GDC, ESB/GDC, and DWSB/SNDC bilayers. Total electrolyte thickness is fixed at 10 μm.

reaction (ORR) at the cathode mainly due to the high bond strength of the oxygen molecule,[60–63] while the hydrogen oxidation process in the anode is several orders of magnitude faster than ORR at the cathode. For example, the dissociated chemisorption of hydrogen at the anode is much faster and independent of changing temperature,[63,64] while the cathode ORR is a thermally activated process. Therefore, as operational temperature decreases, increasing non-ohmic polarization in SOFCs is attributable primarily to cathodic polarization. Recent development of high performance cathodes for LT-SOFC has focused on increasing triple phase boundary (TPB) density by microstructural tailoring and/or using highly electrocatalytic materials. Two popular choices for cathode materials are $La_{1-x}Sr_xMnO_{3-\delta}$ (LSM) and $La_{1-x}Sr_xCo_{1-y}Fe_yO_{3-\delta}$ (LSCF) with the perovskite (ABO_3) crystal structures.

LSM-based materials are almost purely p-type electronic conductors with high thermal and chemical stability as well as reasonable catalytic activity for oxygen reduction at high temperature.[65–68] However, due to their negligible bulk ionic conduction and high activation energy, the electrochemical reaction sites (TPBs) are restricted to the electrolyte/cathode interface. Moreover, their sluggish ORRs significantly impact cell performance at lower temperatures.[69] To deal with this issue, composite cathodes have been explored by adding an ionic conductor such as stabilized zirconia and doped ceria. These composites show higher performance at lower temperatures due to improved ionic conduction and enlarged TPB density in three dimensions (3D).[70,71]

In contrast, LSCF is a MIEC resulting in an intrinsically extended TPB region. This plus LSCF's significantly faster

https://doi.org/10.1557/jmr.2012.194 Published online by Cambridge University Press

ORR kinetics result in much higher performance than that of LSM-based cathodes at lower temperatures.[72–74]

In addition to material properties, cathode performance strongly depends on microstructure.[75] Recently, significant effort has been undertaken to achieve high TPB density with a spatially well-percolated distribution of ionic and electronic phases in the cathode bulk and more importantly near cathode/electrolyte interfacial region. One of the successful approaches is infiltration of catalyst precursor solutions forming nanosized particles of electronic (or ionic) conductors on an ionic (or electronic) conducting skeleton structure resulting in significantly increased TPB lengths.[76] Various nanostructured cathode materials have also been explored using synthesis techniques such as wet chemical combustion methods effectively leading to reduced cathodic polarization. In a recent report by Baque et al.,[77] e.g., a nanostructured LSCF cathode prepared by a wet chemical route exhibited ASRs of 0.05 and 0.4 Ωcm^2 at 600 and 450 °C, respectively.

While tailored cathode microstructures have improved cathode performance at lower temperatures, the relation between cathode structure and the oxygen reaction mechanisms in them has not been clearly explained yet. This is due to the complexity of the ORR mechanism and the high randomness of the cathode cermet structure. To deal with this issue, quantification of cathode microstructures has progressed from measuring impedance of well-defined microelectrodes to stereological techniques using analysis of two-dimensional (2D) micrographs.[78–80] Despite some progress in these efforts, the accuracy of measuring practical cathode properties has been limited by overly simplified/unrealistic electrode design, or difficulties to quantify phase interconnectivity which are important to evaluate core microstructural factors linked to electrochemical performance in the cathode such as active TPB density and pore tortuosity.

Recently, new analytical techniques have been used to scrutinize the SOFC cathode structure. Using a focused ion beam (FIB)/scanning electron microscope (SEM) dual beam system, an accurate and realistic cathode structure was successfully reconstructed in 3D and the critical structural properties quantified.[81–87] For the last several years, we have investigated two popular perovskite cathodes: LSM and LSCF (and their composites) cathodes by this state-of-the-art technique. As shown in Fig. 9, we first reported a FIB/SEM 3D reconstruction of a porous LSFC cathode by automated sectioning, alignment, and segmentation of a series of 2D images.[82] From this reconstruction, we successfully quantified the critical microstructural parameters including closed/graded porosity, surface area, tortuosity, and TPB length.

More recently, we demonstrated for the first time a direct relation between quantified microstructural features of "real" LSM porous cathodes and activation polarization mechanisms,[83] using the 3D reconstruction technique combined with AC impedance spectroscopy. As shown in Fig. 10, charge transfer resistance and the adsorption polarization have a power law relationship with TPB density (L_{TPB}) and surface area (S_v), respectively, quantified using FIB/SEM 3D reconstruction. This quantification and deconvolution of the diverse polarization contributions to the cathodic polarization is an important step to the rational design of higher performance cathodes.

Rational design further requires mechanistic understanding of oxygen reduction kinetics on SOFC cathode materials and the role it plays in apparent rate-limiting steps. To achieve this, we utilized heterogeneous catalysis techniques of temperature-programmed desorption, reaction, and isotope exchange, the later using oxygen isotope tracers (O_2^{18}) (Fig. 11).[72,88,89] These studies revealed that the rate-limiting step for LSM is primarily the incorporation of adsorbed oxygen species into the lattice, while for LSCF, it is the dissociative adsorption of oxygen molecules. Moreover, these experiments demonstrated faster ORR kinetics for LSCF with both lower oxygen exchange onset temperature (200 versus 350 °C) and activation energy (0.10 eV versus 0.9 eV at 700 °C) than LSM. The fundamental reaction rate constants from these independent cathode material studies can be combined with the quantified microstructures and electrochemical measurements to provide a more foundational logically based framework for cathode development to further reduce cathode polarization and thus SOFC operation temperature.

B. Development of novel cathode materials

For further improvement of cathode performance at lower temperatures, new cathode materials are continually being explored by many researchers. For example, Shao and Haile[90] reported a high performance cubic perovskite cathode—$Ba_{0.5}Sr_{0.5}Co_{0.8}Fe_{0.2}O_{3-\delta}$ (BSCF) with low ASRs of ~0.06 and ~0.55 Ωcm^2 at 600 and 500 °C, respectively. Thus, these perovskite cathodes (LSCF, BSCF) have been popular choices for LT-SOFCs. However, cobaltite-based materials are reactive with stabilized bismuth oxide, which is an essential component for our bismuth oxide/ceria bilayered electrolyte.

Therefore, we investigated a bismuth oxide compatible high performance low temperature cathode material—a pyrochlore structured bismuth ruthenate ($Bi_2Ru_2O_7$, BRO7).[91,92] Ruthenium oxide is known for its highly catalytic activity. Moreover, Lee et al.[93] have reported that using an A-site dopant with sufficiently large ionic radius, such as Bi or Pb, ruthenium pyrochlores ($A_2Ru_2O_7$) become metallic due to the altered energy band structure by increasing the Ru–O–Ru bond angle. Thus, when using these materials with Bi as the A-site dopant, high electronic conduction is expected at low temperatures. Our initial results demonstrated that BRO7 is compatible with both

https://doi.org/10.1557/jmr.2012.194 Published online by Cambridge University Press

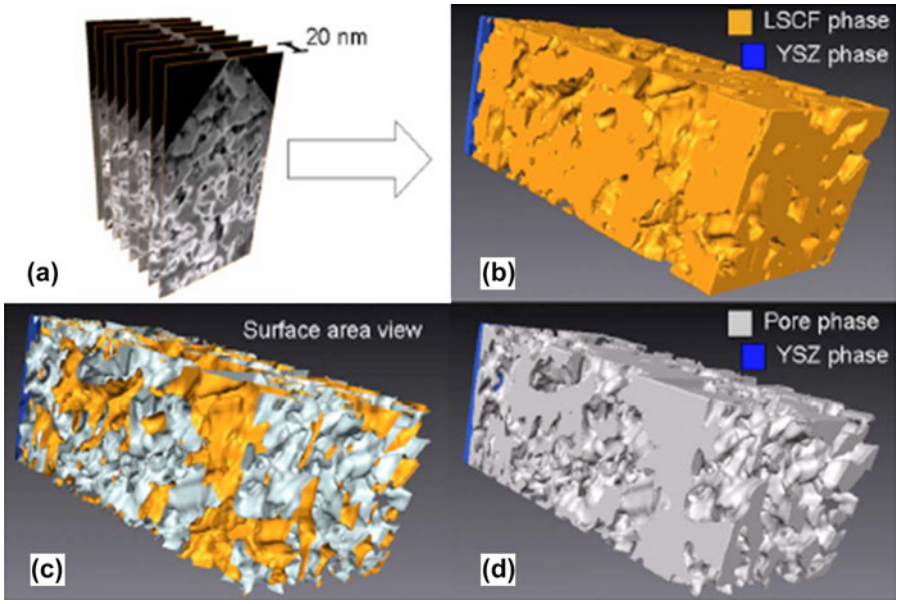


FIG. 9. (a) SEM 2D images were stacked, aligned, and reconstructed into (b) a 3D triangular mesh representing actual LSCF/YSZ interfacial microstructure sintered at 950 °C. This allows for measurement of (c) surface area and (d) volume porosity.[80]

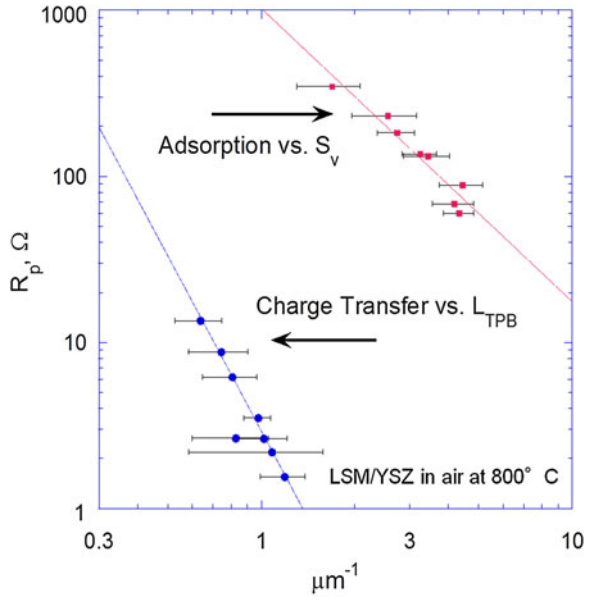


FIG. 10. Effect of LSM microstructure on cathode polarization; dissociative adsorption as a function of pore surface area, and charge transfer polarization as a function of triple phase boundary length; at 800 °C in air.[81]

doped ceria and stabilized bismuth oxide and showed reasonably high performance at lower temperatures.[91] Based on this result, we developed a composite cathode consisting of BRO7 as an electronic conducting phase and ESB as ionic conducting phase working on an ESB electrolyte.[19] Previous results with Ag–ESB composite cathodes demonstrated the role of cathode microstructure on electrode polarization and long-term stability of Bi_2O_3 based cathodes.[94,95] Thus, to reduce the electrode polarization of the BRO7–ESB cathode, the effects of two phase composition, microstructural optimization of particle size and distribution for each phase, and the electrode thickness were investigated (Fig. 12),[20] resulting in electrode ASRs of BRO7–ESB composite cathodes on ESB electrolytes of only 0.03 and 0.73 Ωcm^2 at 700 and 500 °C, respectively. This result is comparable to the performance of the state-of-the-art BSCF cathode, particularly at lower temperatures due to low activation energy of BRO7–ESB cathodes.

IV. DEVELOPMENT OF HIGH PERFORMANCE ANODES FOR LT-SOFCs

A. Anode-supported design and anode functional layers for LT-SOFCs

To minimize ohmic resistance and promote higher power density at lower temperatures, the electrolyte thickness should be reduced. One of the most successful approaches has been to use an anode-supported cell architecture, which can accommodate very thin electrolytes (~10 μm).[96,97]

These are typically tape cast anode supports, which in our case are comprised of a mixture of large-sized (over several micrometers) NiO particles and submicron-sized GDC powders.[51,98] Under operating conditions, reduction of large NiO into Ni metal produces porosity. The measured value is around ~30% porosity. Figure 13 shows the tape cast anode-supported cells, which we typically fabricate, from the green tape to the sintered body with a thin GDC electrolyte layer. The shrinkage rate of the diameter during sintering is about 15% (from 3.18 to 2.70 cm).

https://doi.org/10.1557/jmr.2012.194 Published online by Cambridge University Press

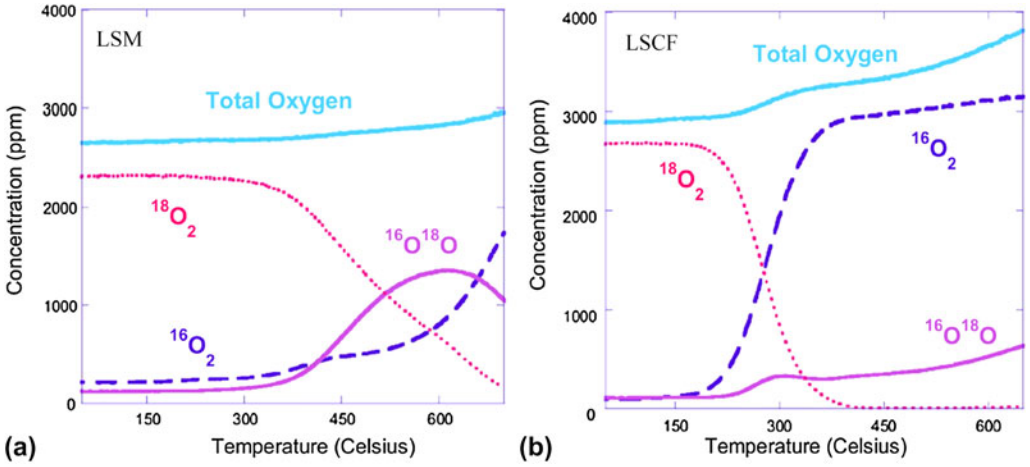


FIG. 11. Temperature-programmed isotope exchange for (a) LSM and (b) LSCF.[72]

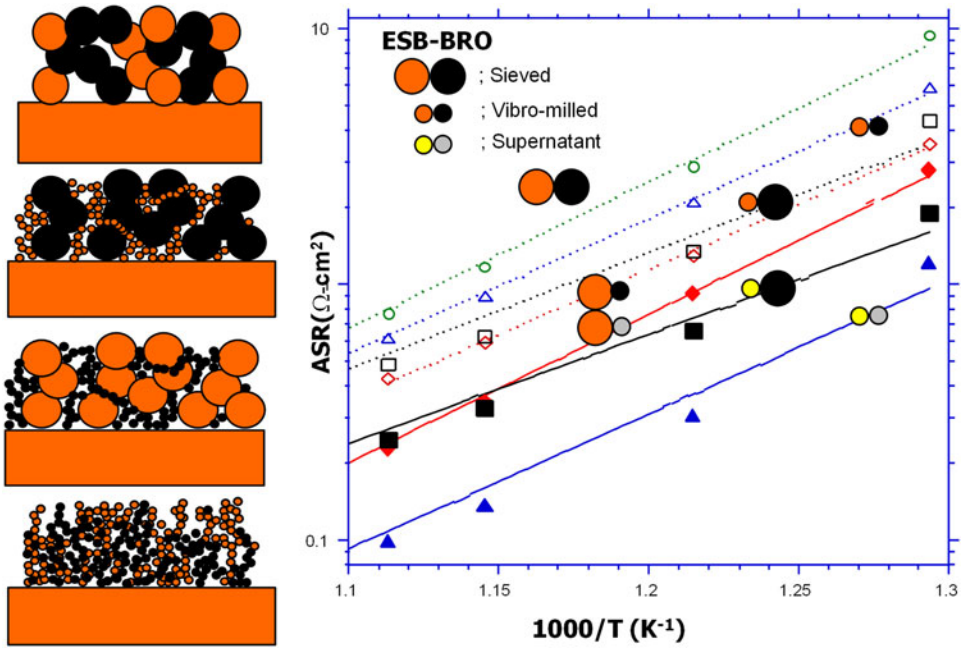


FIG. 12. Mircrostructural optimization and performance of bismuth ruthenate–bismuth oxide (BRO7–ESB) composite cathode.[20]

For high performance, anode supports should equip two main functionalities. First is a large pore microstructure to accommodate rapid gas transport, both fuel in and reaction by-products, such as water, out. Second is a high surface area triple phase boundary region to maximize anodic reactions. In many cases, a mixture of submicron-sized anode powder and pore former are used for the anode support.[99,100] Therefore, there is a trade-off between the desired porosity and TPB density in anode structures. Moreover, high porosity anodes can cause insufficient mechanical stability and poor interfacial contact between the anode and electrolyte.[99] Thus, to increase the number of anode reaction sites and reduce abrupt microstructural change at the anode/electrolyte interface, various anode functional layers (AFLs) with finer microstructure have been developed.[100–104]

We use an AFL at the electrolyte/anode interface by dispersing very fine GDC particles using a precursor solution.[98] After heat treatment, the nanosized GDC particles fill pores at the anode/electrolyte interface, improving the quality of electrolyte deposition resulting in higher OCP and lower ohmic ASR. In addition, fine particles penetrate into the anode bulk increasing TPB and a significant anodic polarization decrease. A SOFC with GDC–AFL was tested at temperature ranging from 650 °C down to 450 °C. The resultant total ASR was only 0.089 Ωcm^2 at 650 °C, and the MPDs reached ~1 W/cm^2 at 650 °C and ~0.24 W/cm^2 at 450 °C (Fig. 14). However, impedance analysis revealed

https://doi.org/10.1557/jmr.2012.194 Published online by Cambridge University Press

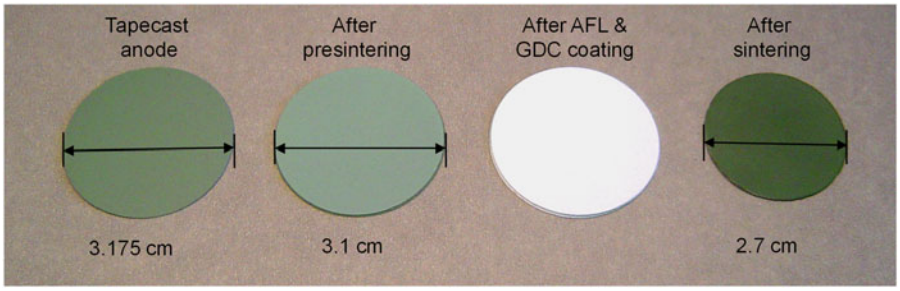


FIG. 13. Fabrication of an anode-supported SOFC from a tape cast anode to a sintered button cell. After sintering, the lateral shrinkage rate is about 15%.

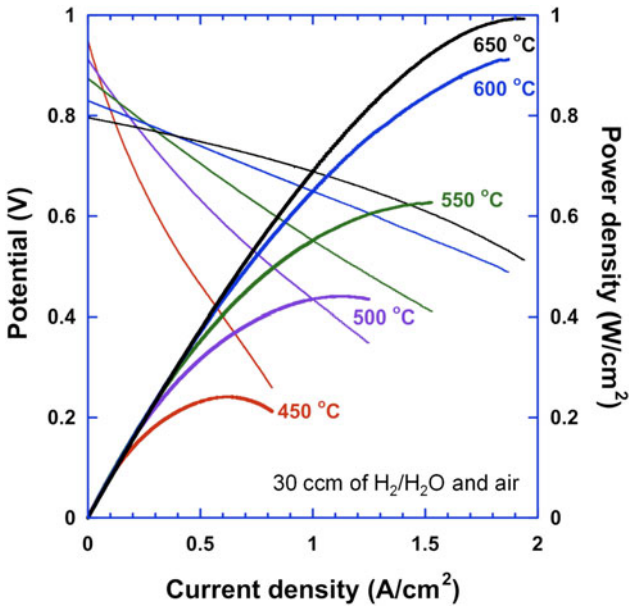


FIG. 14. I–V characteristics of anode-supported GDC SOFC with AFL and LSCF/GDC cathode from 450 to 650 °C under 30 sccm of wet hydrogen and air.[96]

that the electrode ASR was still dominant at lower temperature, ~73% of total cell resistance at 450 °C.

For further improvement, we developed an AFL structure integrating different size particles with cost-effective fabrication processes, yielding power densities of ~1.13 and 1.29 W/cm^2 at 600 and 650 °C, respectively.[105] Moreover, the effect of AFL composition on microstructure and electrochemical performance was investigated and we found the optimal composition range of Ni–GDC AFL as a ~1:1 volume ratio.[51]

B. Investigation of anodes for hydrocarbon fuels

In principle, the relatively high operating temperature (>~600 °C) of SOFCs compared to other types of FCs enables internal reforming and the ability to operate on a variety of hydrocarbon fuels. However, as operating temperature decreases, the most widely used Ni–YSZ cermet anodes, under hydrocarbon fuel conditions, have shown carbon deposition and sulfur (a common impurity in most hydrocarbon fuels) poisoning on the surface of the Ni catalyst, leading to significant power output decay.[106]

Various approaches have been developed for effective suppression of coking (carbon deposition) and sulfur poisoning. For example, Murray et al.[107] reported the direct electrochemical oxidation of methane in SOFCs using a thin $(Y_2O_3)_{0.15}(CeO_2)_{0.85}$ layer (~0.5 μm) between the YSZ electrolyte and Ni–YSZ anode. With the aid of additional ceria catalysts, coking was suppressed at the Ni–YSZ anode, with a MPD of 0.37 W/cm^2 at 650 °C. Similarly, Zhan and Barnett[108] utilized a thin Ru–CeO_2 catalyst layer on top of the Ni–YSZ anode. Using this configuration, they demonstrated internal reforming of isooctane with greater coking resistance, generating stable power densities up to 0.6 W/cm^2 at 770 °C. Recently, Yang et al.[109] developed an enhanced coking and sulfur resistant anode comprised of $BaZr_{0.1}Ce_{0.7}Y_{0.2-x}Yb_xO_{3-\delta}$ (BZCYYb) as a replacement for the ionic conducting phase in Ni–YSZ cermet. They reported that the Ni–BZCYYb cermet anode had excellent hydrocarbon reforming and sulfur oxidation ability up to 50 ppm of H_2S due to the mixed transport of both protons and oxide vacancies enhancing catalytic activity and water adsorption at low temperature, 500–700 °C. Using a SOFC with Ni–BZCYYb/BZCYYb/BZCYYb–LSCF, the MPD obtained reached ~1.1 W/cm^2 at 750 °C.

Another approach is to replace the Ni, which is susceptible to coking and sulfur poisoning with alternative electronic conducting phases. Park et al.,[110] e.g., developed composite anodes of Cu–CeO_2 (or doped ceria)–YSZ. Due to the low melting temperature of copper (<~1100 °C), the composite anode was fabricated by infiltrating a porous YSZ scaffold with precursor solutions containing the constituent ions.[111] During SOFC operation, these composite anodes allowed the direct utilization of a variety of hydrocarbon fuels, ranging from methane to toluene, and exhibited very high coking resistance and sulfur tolerance (up to ~400 ppm) without serious performance degradation. In this anode design, copper works mainly as an electronic conductor and ceria (or doped ceria) plays a catalytic role for fuel reforming and oxidation. Similarly,

https://doi.org/10.1557/jmr.2012.194 Published online by Cambridge University Press

all ceramic anodes have been investigated, such as perovskites $La_{0.75}Sr_{0.25}Cr_{0.5}Mn_{0.5}O_3$,[112] $La_{0.4}Sr_{0.6}Ti_{1-x}Mn_xO_3$,[113] and double perovskite $Sr_2Mg_{1-x}Mn_xMoO_{6-\delta}$.[114] Despite progress on coking resistance and sulfur tolerance with hydrocarbon fuels, further improvement is necessary as these alternative anodes have relatively low performance compared to Ni-based cermet anodes due to lower conductivity and catalytic activity.

One thing appears clear in these studies that ceria-based anodes have greater coking resistance and sulfur tolerance than zirconia-based anodes. This is due to both greater ionic conductivity and more facile $Ce^{3+/4+}$ redox behavior. Recently, we operated our micron-sized Ni–GDC anode-supported SOFC with submicron-sized Ni–GDC AFL cells on JP5 diesel reformate (1.1% CH_4, 12.3% CO, 12.3% CO_2, 40.5% H_2, and 24.5% H_2O balanced with N_2) at 550–650 °C resulting in less than 30% decrease in power densities compared to pure hydrogen (3% humidified) fuel [Fig. 15(a)]. Moreover, during long-term stability tests with JP5 reformate at 550 °C, after an initial decay in first 100 h, there was no measurable degradation up to 500 h [Fig. 15(b)].[115] This is important because ~600 °C is considered as a lower temperature limit for internal reforming without coking for Ni anodes and demonstrates the beneficial effect of replacing YSZ with GDC in the active AFL region. However, further work is necessary with pure methane or higher hydrocarbons due to greater carbon deposition tendency by Boudouard reaction (disproportionation of carbon monoxide)[107] and higher susceptibility to sulfur poisoning at lower temperatures. Moreover, for SOFC operation below 500 °C, it will be necessary to develop and integrate an external fuel processor to partially reform/oxidize the fuel prior to entering the anode.

V. HIGH PERFORMANCE LT-SOFC—INTEGRATING COMPONENTS

By integrating several of the innovations described above, we designed an anode-supported cell with an AFL, a thin ESB/GDC bilayered electrolyte, and a BRO7–ESB cathode.[21] The different sintering temperatures between stabilized bismuth oxide (~900 °C) and doped ceria

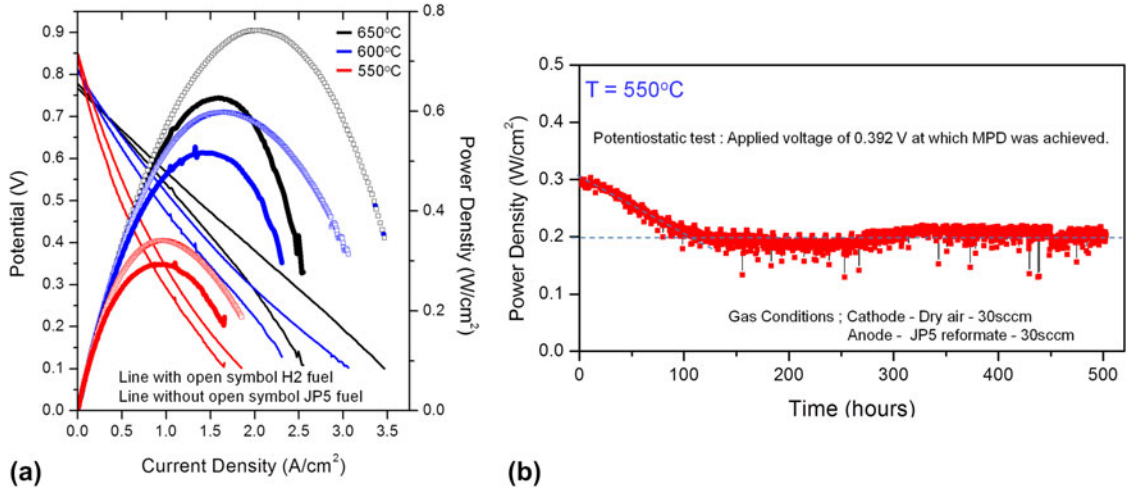


FIG. 15. (a) Current–voltage behavior of SOFCs with H_2 and JP5 reformate fuel from 500 to 650 °C. (b) Long-term stability test of the SOFC on JP5 reformate at 550 °C for 500 h.[113]

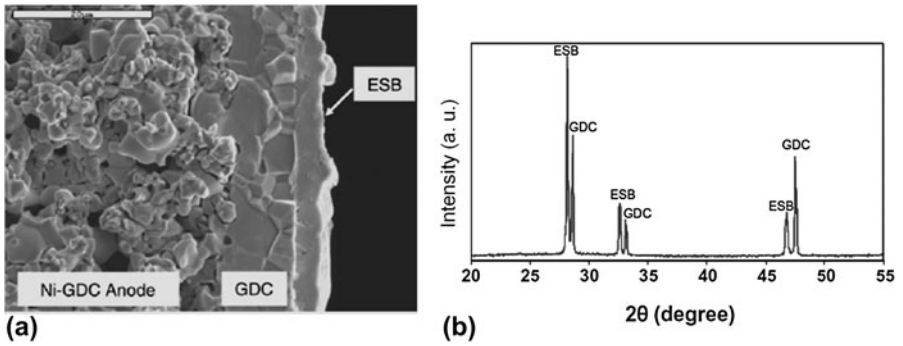


FIG. 16. (a) SEM image of the cross section of the ESB/GDC bilayer electrolyte on Ni–GDC anode support. Pulsed laser deposition of ESB on GDC resulted in a 4-μm-thick film. (b) XRD pattern of the as-deposited bilayer sample.[22]

https://doi.org/10.1557/jmr.2012.194 Published online by Cambridge University Press

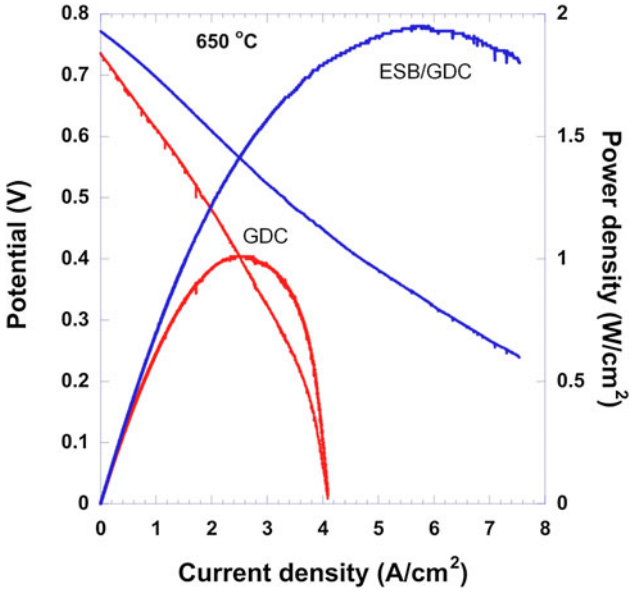


FIG. 17. I–V characteristics of the FC samples with GDC single-layer and ESB/GDC bilayered electrolyte at 650 °C using 90 sccm of air and wet hydrogen.[22]

(~1500 °C) make it nontrivial to deposit a dense ESB layer on the GDC surface using conventional powder copressing or colloidal deposition processes. To solve this issue, we used pulsed laser deposition and successfully established a thin (~4 μm) and dense ESB on 10-μm-thick anode-supported GDC electrolyte (Fig. 16). As explained above, utilization of the thin ESB/GDC bilayer not only increased OCP but also resulted in low ohmic ASR (~0.046 Ωcm^2) at 650 °C. In addition, coupling the enhanced surface oxygen exchange rate of stabilized bismuth oxide, with the highly electrocatalytic and conductive, BRO7–ESB cathode reduced electrode ASR by 48% compared to that of our similarly prepared cells with LSCF–GDC cathode on GDC electrolyte and a total cell ASR (0.079 Ωcm^2) reduction of ~40%. This dramatic electrode ASR reduction is attributed not only to the high performance bismuth ruthenate cathode but also to the enhanced oxygen incorporation rate of ESB at the cathode/electrolyte interface.[116] Finally, as shown in Fig. 17, we obtained a power density of ~2 W/cm^2 at 650 °C, which is 93% increase in MPD compared to that of a GDC single-layer cell (~1.03 W/cm^2)[21,22] and the highest power density achieved in this temperature range (<700 °C). Based on a ~1.5-mm interconnect thickness per planar cell, this corresponds to a stack volumetric power density of ~10 W/cm^3. Further, by including the corresponding densities, we calculate a gravimetric power density for the stack of ~3 kW/kg, greater than that of an IC engine.[1]

VI. CONCLUDING REMARKS

Based on the fundamental understanding of ionic transport of solid electrolytes and heterogeneous electrocatalysis, we have developed various compatible high performance SOFC components: functionally graded ceria/bismuth oxide bilayered electrolytes, bismuth ruthenate-based cathodes, and AFLs. These materials were integrated into an anode-supported cell achieving a power density of ~2 W/cm^2 at 650 °C. We expect to achieve even higher power density at lower temperatures by further reducing electrolyte polarization and by transitioning from the ESB/GDC bilayered electrolyte to the more conductive DWSB/SNDC electrolytes we recently developed. Moreover, with these exceptionally high power densities, we can readily accommodate a decrease in power associated with operating the SOFCs at temperatures of 300–500 °C, opening up the opportunity to use nanostructured electrodes, conventional stainless steel interconnects, and balance of plant (BOP), as well as simple elastomeric seals, reducing system cost and increasing reliability.[1] In addition, the ability to operate on conventional fuels at lower temperatures precludes the requirements for a hydrogen infrastructure that have relegated FCs to a "future technology." Thus, LT-SOFCs are a practical transformational energy conversion technology with the ability for "current market" penetration.

REFERENCES

1. E.D. Wachsman and K.T. Lee: Lowering the temperature of solid oxide fuel cells. *Science* **334**, 935 (2011).
2. E.D. Wachsman, C.A. Marlowe, and K.T. Lee: Role of solid oxide fuel cells in a balanced energy strategy. *Energy Environ. Sci.* **5**, 5498 (2012).
3. B.C.H. Steele: Material science and engineering: The enabling technology for the commercialisation of fuel cell systems. *J. Mater. Sci.* **36**, 1053 (2001).
4. E.D. Wachsman, N. Jiang, D.M. Mason, and D.A. Stevenson: Solid state oxygen kinetics in Er_2O_3 stabilized Bi_2O_3. *Proc. Electrochem. Soc.* **89**, 15 (1989).
5. E.D. Wachsman, N. Jiang, C.W. Frank, D.M. Mason, and D.A. Stevenson: Spectroscopic investigation of oxygen vacancies in solid oxide electrolytes. *Appl. Phys. A: Mater. Sci. Process.* **50**, 545 (1990).
6. E.D. Wachsman, G.R. Ball, N. Jiang, and D.A. Stevenson: Structural and defect studies in solid oxide electrolytes. *Solid State Ionics* **52**, 213 (1992).
7. N. Jiang, R.M. Buchanan, F.E.G. Henn, A.F. Marshall, D.A. Stevenson, and E.D. Wachsman: Aging phenomenon of stabilized bismuth oxides. *Mater. Res. Bull.* **29**, 247 (1994).
8. N.X. Jiang and E.D. Wachsman: Structural stability and conductivity of phase-stabilized cubic bismuth oxides. *J. Am. Ceram. Soc.* **82**, 3057 (1999).
9. E.D. Wachsman, S. Boyapati, M.J. Kaufman, and N.X. Jiang: Modeling of ordered structures of phase-stabilized cubic bismuth oxides. *J. Am. Ceram. Soc.* **83**, 1964 (2000).
10. S. Boyapati, E.D. Wachsman, and N.X. Jiang: Effect of oxygen sublattice ordering on interstitial transport mechanism and conductivity activation energies in phase-stabilized cubic bismuth oxides. *Solid State Ionics* **140**, 149 (2001).
11. S. Boyapati, E.D. Wachsman, and B.C. Chakoumakos: Neutron diffraction study of occupancy and positional order of oxygen ions in phase stabilized cubic bismuth oxides. *Solid State Ionics* **138**, 293 (2001).

https://doi.org/10.1557/jmr.2012.194 Published online by Cambridge University Press

12. E.D. Wachsman, S. Boyapati, and N. Jiang: Effect of dopant polarizability on oxygen sublattice order in phase-stable cubic bismuth oxide. *Ionics* **7**, 6 (2001).
13. N.X. Jiang, E.D. Wachsman, and S.H. Jung: A higher conductivity Bi_2O_3-based electrolyte. *Solid State Ionics* **150**, 347 (2002).
14. E.D. Wachsman: Effect of oxygen sublattice order on conductivity in highly defective fluorite oxides. *J. Eur. Ceram. Soc.* **24**, 1281 (2004).
15. D.W. Jung, K.L. Duncan, and E.D. Wachsman: Effect of total dopant concentration and dopant ratio on conductivity of $(DyO_{1.5})_x$-$(WO_3)_y$-$(BiO_{1.5})_{1-x-y}$. *Acta Mater.* **58**, 355 (2010).
16. D.W. Jung, J.C. Nino, K.L. Duncan, S.R. Bishop, and E.D. Wachsman: Enhanced long-term stability of bismuth oxide-based electrolytes for operation at 500 A degrees C. *Ionics* **16**, 97 (2010).
17. D.W. Jung, K.L. Duncan, M.A. Camaratta, K.T. Lee, J.C. Nino, and E.D. Wachsman: Effect of annealing temperature and dopant concentration on the conductivity behavior in $(DyO_{1.5})_x$-$(WO_3)_y$-$(BiO_{1.5})_{1-x-y}$. *J. Am. Ceram. Soc.* **93**, 1384 (2010).
18. E.D. Wachsman, P. Jayaweera, N. Jiang, D.M. Lowe, and B.G. Pound: Stable high conductivity ceria/bismuth oxide bilayered electrolytes. *J. Electrochem. Soc.* **144**, 233 (1997).
19. A. Jaiswal, C.T. Hu, and E.D. Wachsman: Bismuth ruthenate-stabilized bismuth oxide composite cathodes for IT-SOFC. *J. Electrochem. Soc.* **154**, B1088 (2007).
20. M. Camaratta and E. Wachsman: High-performance composite $Bi_2Ru_2O_7$-$Bi_{1.6}Er_{0.4}O_3$ cathodes for intermediate-temperature solid oxide fuel cells. *J. Electrochem. Soc.* **155**, B135 (2008).
21. J.S. Ahn, M.A. Camaratta, D. Pergolesi, K.T. Lee, H. Yoon, B.W. Lee, D.W. Jung, E. Traversa, and E.D. Wachsman: Development of high performance ceria/bismuth oxide bilayered electrolyte SOFCs for lower temperature operation. *J. Electrochem. Soc.* **157**, B376 (2010).
22. J.S. Ahn, D. Pergolesi, M.A. Camaratta, H. Yoon, B.W. Lee, K.T. Lee, D.W. Jung, E. Traversa, and E.D. Wachsman: High-performance bilayered electrolyte intermediate temperature solid oxide fuel cells. *Electrochem. Commun.* **11**, 1504 (2009).
23. B.C.H. Steele and A. Heinzel: Materials for fuel-cell technologies. *Nature* **414**, 345 (2001).
24. S. deSouza, S.J. Visco, and L.C. DeJonghe: Thin-film solid oxide fuel cell with high performance at low-temperature. *Solid State Ionics* **98**, 57 (1997).
25. B.C.H. Steele: Interfacial reactions associated with ceramic ion-transport membranes. *Solid State Ionics* **75**, 157 (1995).
26. T. Takahashi, T. Esaka, and H. Iwahara: High oxide ion conduction in sintered oxides of system Bi_2O_3-Gd_2O_3. *J. Appl. Electrochem.* **5**, 197 (1975).
27. H.A. Harwig: Structure of bismuthsesquioxide – alpha, beta, gamma and delta-phase. *Z. Anorg. Allg. Chem.* **444**, 151 (1978).
28. T. Takahashi, T. Esaka, and H. Iwahara: Electrical-conduction in sintered oxides of system Bi_2O_3-BaO. *J. Solid State Chem.* **16**, 317 (1976).
29. M.J. Verkerk, K. Keizer, and A.J. Burggraaf: High oxygen ion conduction in sintered oxides of the Bi_2O_3-Er_2O_3 system. *J. Appl. Electrochem.* **10**, 81 (1980).
30. L.G. Sillen: X-ray studies on bismuth trioxide. *Ark. Kemi Mineral. Geol.* **12A**, 15 (1937).
31. G. Gattow and H. Schröder: About bismuth oxides. III. The crystal structure of the high-temperature modification of bismuth (III) oxide (δ-Bi_2O_3). *Z. Anorg. Allg. Chem.* **318**, 14 (1962).
32. B.T.M. Willis: The anomalous behaviour of the neutron reflexion of fluorite. *Acta Crystallogr.* **18**, 2 (1965).
33. D.S. Aidhy, J.C. Nino, S.B. Sinnott, E.D. Wachsman, and S.R. Phillpot: Vacancy-ordered structure of cubic bismuth oxide from simulation and crystallographic analysis. *J. Am. Ceram. Soc.* **91**, 2349 (2008).
34. D.S. Aidhy, S.B. Sinnott, E.D. Wachsman, S.R. Phillpot, and J.C. Nino: Structure of delta-Bi_2O_3 from density functional theory: A systematic crystallographic analysis. *J. Solid State Chem.* **182**, 1222 (2009).
35. S.N. Hoda and L.L.Y. Chang: Phase relations in system Bi_2O_3-WO_3. *J. Am. Ceram. Soc.* **57**, 323 (1974).
36. A. Watanabe and A. Ono: Thermostable region of an oxide ion conductor, $Bi_7WO_{13.5}$ (=$7Bi_2O_3$ -$2WO_3$), and the solid solubility extension. *Solid State Ionics* **174**, 15 (2004).
37. T. Takahashi, T. Esaka, and H. Iwahara: Conduction in Bi_2O_3-based oxide ion conductors under low oxygen-pressure. 1. Current blackening of Bi_2O_3-Y_2O_3 electrolyte. *J. Appl. Electrochem.* **7**, 299 (1977).
38. C.Z. Wang, X.G. Xu, and B.Z. Li: Ionic and electronic conduction of oxygen ion conductors in the Bi_2O_3-Y_2O_3 system. *Solid State Ionics* **13**, 135 (1984).
39. P. Duran, J.R. Jurado, C. Moure, N. Valverde, and B.C.H. Steele: High oxygen ion conduction in some Bi_2O_3-Y_2O_3(Er_2O_3) solid-solutions. *Mater. Chem. Phys.* **18**, 287 (1987).
40. H. Yahiro, Y. Eguchi, K. Eguchi, and H. Arai: Oxygen ion conductivity of the ceria samarium oxide system with fluorite structure. *J. Appl. Electrochem.* **18**, 527 (1988).
41. K. Eguchi, T. Setoguchi, T. Inoue, and H. Arai: Electrical-properties of ceria-based oxides and their application to solid oxide fuel-cells. *Solid State Ionics* **52**, 165 (1992).
42. B.C.H. Steele: Appraisal of $Ce_{1-y}Gd_yO_{2-y/2}$ electrolytes for IT-SOFC operation at 500 degrees C. *Solid State Ionics* **129**, 95 (2000).
43. S. Omar, E.D. Wachsman, and J.C. Nino: A co-doping approach towards enhanced ionic conductivity in fluorite-based electrolytes. *Solid State Ionics* **177**, 3199 (2006).
44. S. Omar, E.D. Wachsman, and J.C. Nino: Higher ionic conductive ceria-based electrolytes for solid oxide fuel cells. *Appl. Phys. Lett.* **91**, 114106-1–114106-3 (2007).
45. S. Omar, E.D. Wachsman, and J.C. Nino: Higher conductivity Sm^{3+} and Nd^{3+} co-doped ceria-based electrolyte materials. *Solid State Ionics* **178**, 1890 (2008).
46. D.A. Andersson, S.I. Simak, N.V. Skorodumova, I.A. Abrikosov, and B. Johansson: Optimization of ionic conductivity in doped ceria. *Proc. Natl. Acad. Sci. U.S.A.* **103**, 3518 (2006).
47. R.D. Shannon: Revised effective ionic-radii and systematic studies of interatomic distances in halides and chalcogenides. *Acta Crystallogr., Sect. A* **32**, 751 (1976).
48. J.S. Ahn, S. Omar, H. Yoon, J.C. Nino, and E.D. Wachsman: Performance of anode-supported solid oxide fuel cell using novel ceria electrolyte. *J. Power Sources* **195**, 2131 (2010).
49. K.L. Duncan and E.D. Wachsman: Continuum-level analytical model for solid oxide fuel cells with mixed conducting electrolytes. *J. Electrochem. Soc.* **156**, B1030 (2009).
50. S.M. Haile: Fuel cell materials and components. *Acta Mater.* **51**, 5981 (2003).
51. K.T. Lee, N.J. Vito, C.A. Mattehw, H.S. Yoon, and E.D. Wachsman: Effect of Ni-GDC AFL composition on performance of IT-SOFCs. *ECS Trans.* **28**, 151 (2010).
52. D.J.L. Brett, A. Atkinson, N.P. Brandon, and S.J. Skinner: Intermediate temperature solid oxide fuel cells. *Chem. Soc. Rev.* **37**, 1568 (2008).
53. X. Zhang, M. Robertson, C. Deces-Petit, W. Qu, O. Kesler, R. Maric, and D. Ghosh: Internal shorting and fuel loss of a low temperature solid oxide fuel cell with SDC electrolyte. *J. Power Sources* **164**, 668 (2007).
54. K.L. Duncan, K.T. Lee, and E.D. Wachsman: Dependence of open-circuit potential and power density on electrolyte thickness

https://doi.org/10.1557/jmr.2012.194 Published online by Cambridge University Press

in solid oxide fuel cells with mixed conducting electrolytes. *J. Power Sources* **196**, 2445 (2011).
55. J.Y. Park and E.D. Wachsman: Stable and high conductivity ceria/bismuth oxide bilayer electrolytes for lower temperature solid oxide fuel cells. *Ionics* **12**, 15 (2006).
56. E.D. Wachsman: Functionally gradient bilayer oxide membranes and electrolytes. *Solid State Ionics* **152**, 657 (2002).
57. K.T. Lee, D.W. Jung, M.A. Camaratta, J.S. Ahn, and E.D. Wachsman: $Gd_{0.1}Ce_{0.9}O_{1.95}/Er_{0.2}Bi_{1.6}O_3$ bilayered electrolytes fabricated by a simple colloidal route using nano-sized $Er_{0.2}Bi_{1.6}O_3$ powders for high performance LT-SOFCs. *J. Power Sources* **205**, 122 (2012).
58. Q.L. Liu, K.A. Khor, S.H. Chan, and X.J. Chen: Anode-supported solid oxide fuel cell with yttria-stabilized zirconia/gadolinia-doped ceria bilayer electrolyte prepared by wet ceramic co-sintering process. *J. Power Sources* **162**, 1036 (2006).
59. H-T. Lim and A.V. Virkar: Measurement of oxygen chemical potential in Gd_2O_3-doped ceria-Y_2O_3-stabilized zirconia bi-layer electrolyte, anode-supported solid oxide fuel cells. *J. Power Sources* **192**, 267 (2009).
60. C.R. Xia, W. Rauch, F.L. Chen, and M.L. Liu: $Sm_{0.5}Sr_{0.5}CoO_3$ cathodes for low-temperature SOFCs. *Solid State Ionics* **149**, 11 (2002).
61. K. Sasaki, J. Tamura, H. Hosoda, T.N. Lan, K. Yasumoto, and M. Dokiya: Pt-perovskite cermet cathode for reduced-temperature SOM. *Solid State Ionics* **148**, 551 (2002).
62. T. Ishihara, T. Kudo, H. Matsuda, and Y. Takita: Doped $PrMnO_3$ perovskite oxide as a new cathode of solid oxide fuel-cells for low-temperature operation. *J. Electrochem. Soc.* **142**, 1519 (1995).
63. M. Mogensen and S. Skaarup: Kinetic and geometric aspects of solid oxide fuel cell electrodes. *Solid State Ionics* **86–88**, 1151 (1996).
64. M. Godickemeier, K. Sasaki, L.J. Gauckler, and I. Riess: Perovskite cathodes for solid oxide fuel cells based on ceria electrolytes. *Solid State Ionics* **86–88**, 691 (1996).
65. N.Q. Minh: Ceramic fuel-cells. *J. Am. Ceram. Soc.* **76**, 563 (1993).
66. E.P. Murray, T. Tsai, and S.A. Barnett: Oxygen transfer processes in (La, Sr)MnO_3/Y_2O_3-stabilized ZrO_2 cathodes: An impedance spectroscopy study. *Solid State Ionics* **110**, 235 (1998).
67. S.P. Yoon, J. Han, S.W. Nam, T.H. Lim, I.H. Oh, S.A. Hong, Y.S. Yoo, and H.C. Lim: Performance of anode-supported solid oxide fuel cell with $La_{0.85}Sr_{0.15}MnO_3$ cathode modified by sol-gel coating technique. *J. Power Sources* **106**, 160 (2002).
68. S.P. Jiang: Issues on development of (La, Sr)MnO_3 cathode for solid oxide fuel cells. *J. Power Sources* **124**, 390 (2003).
69. N.P. Brandon, S. Skinner, and B.C.H. Steele: Recent advances in materials for fuel cells. *Annu. Rev. Mater. Res.* **33**, 183 (2003).
70. C.W. Tanner, K.Z. Fung, and A.V. Virkar: The effect of porous composite electrode structure on solid oxide fuel cell performance. 1. Theoretical analysis. *J. Electrochem. Soc.* **144**, 21 (1997).
71. E.P. Murray and S.A. Barnett: (La, Sr) MnO_3-(Ce, Gd)O_{2-x} composite cathodes for solid oxide fuel cells. *Solid State Ionics* **143**, 265 (2001).
72. S.P. Jiang: A comparison of O^{-2} reduction reactions on porous (La, Sr)MnO_3 and (La, Sr)(Co, Fe)O_3 electrodes. *Solid State Ionics* **146**, 1 (2002).
73. I. Yasuda, K. Ogasawara, M. Hishinuma, T. Kawada, and M. Dokiya: Oxygen tracer diffusion coefficient of (La, Sr)$MnO_{3+/-delta}$. *Solid State Ionics* **86–88**, 1197 (1996).
74. C.C. Kan, H.H. Kan, F.M. Van Assche, E.N. Armstrong, and E.D. Wachsman: Investigating oxygen surface exchange kinetics of $La_{0.8}Sr_{0.2}MnO_{3-delta}$ and $La_{0.6}Sr_{0.4}Co_{0.2}Fe_{0.8}O_{3-delta}$ using an isotopic tracer. *J. Electrochem. Soc.* **155**, B985 (2008).
75. S.B. Adler: Factors governing oxygen reduction in solid oxide fuel cell cathodes. *Chem. Rev.* **104**, 4791 (2004).
76. J.M. Vohs and R.J. Gorte: High-performance SOFC cathodes prepared by infiltration. *Adv. Mater.* **21**, 943 (2009).
77. L. Baque, A. Caneiro, M.S. Moreno, and A. Serquis: High performance nanostructured IT-SOFC cathodes prepared by novel chemical method. *Electrochem. Commun.* **10**, 1905 (2008).
78. J.R. Wilson and S.A. Barnett: Solid oxide fuel cell Ni-YSZ anodes: Effect of composition on microstructure and performance. *Electrochem. Solid-State Lett.* **11**, B181 (2008).
79. N. Shikazono, Y. Sakamoto, Y. Yamaguchi, and N. Kasagi: Microstructure and polarization characteristics of anode supported tubular solid oxide fuel cell with co-precipitated and mechanically mixed Ni-YSZ anodes. *J. Power Sources* **193**, 530 (2009).
80. A. Bieberle, L.P. Meier, and L.J. Gauckler: The electrochemistry of Ni pattern anodes used as solid oxide fuel cell model electrodes. *J. Electrochem. Soc.* **148**, A646 (2001).
81. J.R. Wilson, W. Kobsiriphat, R. Mendoza, H.Y. Chen, J.M. Hiller, D.J. Miller, K. Thornton, P.W. Voorhees, S.B. Adler, and S.A. Barnett: Three-dimensional reconstruction of a solid-oxide fuel-cell anode. *Nat. Mater.* **5**, 541 (2006).
82. D. Gostovic, J.R. Smith, D.P. Kundinger, K.S. Jones, and E.D. Wachsman: Three-dimensional reconstruction of porous LSCF cathodes. *Electrochem. Solid-State Lett.* **10**, B214 (2007).
83. J.R. Smith, A. Chen, D. Gostovic, D. Hickey, D. Kundinger, K.L. Duncan, R.T. DeHoff, K.S. Jones, and E.D. Wachsman: Evaluation of the relationship between cathode microstructure and electrochemical behavior for SOFCs. *Solid State Ionics* **180**, 90 (2009).
84. J.R. Wilson, A.T. Duong, M. Gameiro, H.Y. Chen, K. Thornton, D.R. Mumm, and S.A. Barnett: Quantitative three-dimensional microstructure of a solid oxide fuel cell cathode. *Electrochem. Commun.* **11**, 1052 (2009).
85. J.R. Wilson, M. Gameiro, K. Mischaikow, W. Kalies, P.W. Voorhees, and S.A. Barnett: Three-dimensional analysis of solid oxide fuel cell Ni-YSZ anode interconnectivity. *Microsc. Microanal.* **15**, 71 (2009).
86. J.R. Wilson, J.S. Cronin, A.T. Duong, S. Rukes, H.Y. Chen, K. Thornton, D.R. Mumm, and S. Barnett: Effect of composition of ($La_{0.8}Sr_{0.2}MnO_3$-Y_2O_3-stabilized ZrO_2) cathodes: Correlating three-dimensional microstructure and polarization resistance. *J. Power Sources* **195**, 1829 (2010).
87. N. Shikazono, D. Kanno, K. Matsuzaki, H. Teshima, S. Sumino, and N. Kasagi: Numerical assessment of SOFC anode polarization based on three-dimensional model microstructure reconstructed from FIB-SEM images. *J. Electrochem. Soc.* **157**, B665 (2010).
88. C.C. Kan and E.D. Wachsman: Identifying drivers of catalytic activity through systematic surface modification of cathode materials. *J. Electrochem. Soc.* **156**, B695 (2009).
89. C.C. Kan and E.D. Wachsman: Isotopic-switching analysis of oxygen reduction in solid oxide fuel cell cathode materials. *Solid State Ionics* **181**, 338 (2010).
90. Z.P. Shao and S.M. Haile: A high-performance cathode for the next generation of solid-oxide fuel cells. *Nature* **431**, 170 (2004).
91. A. Jaiswal and E.D. Wachsman: Bismuth-ruthenate-based cathodes for IT-SOFCs. *J. Electrochem. Soc.* **152**, A787 (2005).
92. A. Jaiswal and E. Wachsman: Impedance studies on bismuth-ruthenate-based electrodes. *Ionics* **15**, 1 (2009).
93. K.S. Lee, D.K. Seo, and M.H. Whangbo: Structural and electronic factors governing the metallic and nonmetallic properties of the pyrochlores $A_2Ru_2O_{7-y}$. *J. Solid State Chem.* **131**, 405 (1997).
94. M. Camaratta and E. Wachsman: Silver-bismuth oxide cathodes for IT-SOFCs - Part II - Improving stability through microstructural control. *Solid State Ionics* **178**, 1411 (2007).
95. M. Camaratta and E. Wachsman: Silver-bismuth oxide cathodes for IT-SOFCs; Part I - Microstructural instability. *Solid State Ionics* **178**, 1242 (2007).

https://doi.org/10.1557/jmr.2012.194 Published online by Cambridge University Press

96. J. Will, A. Mitterdorfer, C. Kleinlogel, D. Perednis, and L.J. Gauckler: Fabrication of thin electrolytes for second-generation solid oxide fuel cells. *Solid State Ionics* **131**, 79 (2000).
97. J.W. Kim, A.V. Virkar, K.Z. Fung, K. Mehta, and S.C. Singhal: Polarization effects in intermediate temperature, anode-supported solid oxide fuel cells. *J. Electrochem. Soc.* **146**, 69 (1999).
98. J.S. Ahn, H. Yoon, K.T. Lee, M.A. Camaratta, and E.D. Wachsman: Performance of IT-SOFC with $Ce_{0.9}Gd_{0.1}O_{1.95}$ functional layer at the interface of $Ce_{0.9}Gd_{0.1}O_{1.95}$ electrolyte and Ni-$Ce_{0.9}Gd_{0.1}O_{1.95}$ anode. *Fuel Cells* **9**, 643 (2009).
99. N. Ai, Z. Lu, K.F. Chen, X.Q. Huang, X.B. Du, and W.H. Su: Effects of anode surface modification on the performance of low temperature SOFCs. *J. Power Sources* **171**, 489 (2007).
100. J.J. Haslam, A.Q. Pham, B.W. Chung, J.F. DiCarlo, and R.S. Glass: Effects of the use of pore formers on performance of an anode supported solid oxide fuel cell. *J. Am. Ceram. Soc.* **88**, 513 (2005).
101. N. Ai, Z. Lu, J.K. Tang, K.F. Chen, X.Q. Huang, and W.H. Su: Improvement of output performance of solid oxide fuel cell by optimizing Ni/samaria-doped ceria anode functional layer. *J. Power Sources* **185**, 153 (2008).
102. D. Stover, H.P. Buchkremer, and S. Uhlenbruck: Processing and properties of the ceramic conductive multilayer device solid oxide fuel cell (SOFC). *Ceram. Int.* **30**, 1107 (2004).
103. S.D. Kim, S.H. Hyun, J. Moon, J.H. Kim, and R.H. Song: Fabrication and characterization of anode-supported electrolyte thin films for intermediate temperature solid oxide fuel cells. *J. Power Sources* **139**, 67 (2005).
104. E. Wanzenberg, F. Tietz, P. Panjan, and D. Stover: Influence of pre- and post-heat treatment of anode substrates on the properties of DC-sputtered YSZ electrolyte films. *Solid State Ionics* **159**, 1 (2003).
105. K.T. Lee, H.S. Yoon, J.S. Ahn, and E.D. Wachsman: Bimodally integrated Ni-$Gd_{0.1}Ce_{0.9}O_{1.95}$ anode functional layer for lower temperature SOFCs. *Int. J. Hydrogen Energy* (2012, submitted).
106. C.W. Sun and U. Stimming: Recent anode advances in solid oxide fuel cells. *J. Power Sources* **171**, 247 (2007).
107. E.P. Murray, T. Tsai, and S.A. Barnett: A direct-methane fuel cell with a ceria-based anode. *Nature* **400**, 649 (1999).
108. Z.L. Zhan and S.A. Barnett: An octane-fueled solid oxide fuel cell. *Science* **308**, 844 (2005).
109. L. Yang, S.Z. Wang, K. Blinn, M.F. Liu, Z. Liu, Z. Cheng, and M.L. Liu: Enhanced sulfur and coking tolerance of a mixed ion conductor for SOFCs: $BaZr_{0.1}Ce_{0.7}Y_{0.2-x}Yb_xO_{3-delta}$. *Science* **326**, 126 (2009).
110. S.D. Park, J.M. Vohs, and R.J. Gorte: Direct oxidation of hydrocarbons in a solid-oxide fuel cell. *Nature* **404**, 265 (2000).
111. R.J. Gorte and J.M. Vohs: Nanostructured anodes for solid oxide fuel cells. *Curr. Opin. Colloid Interface Sci.* **14**, 236 (2009).
112. J. Pena-Martinez, D. Marrero-Lopez, J.C. Ruiz-Morales, C. Savaniu, P. Nunez, and J.T.S. Irvine: Anodic performance and intermediate temperature fuel cell testing of $La_{0.75}Sr_{0.25}Cr_{0.5}Mn_{0.5}O_{3-delta}$ at lanthanum gallate electrolytes. *Chem. Mater.* **18**, 1001 (2006).
113. Q.X. Fu, F. Tietz, and D. Stover: $La_{0.4}Sr_{0.6}Ti_{1-x}Mn_xO_{3-delta}$ perovskites as anode materials for solid oxide fuel cells. *J. Electrochem. Soc.* **153**, D74 (2006).
114. Y.H. Huang, R.I. Dass, Z.L. Xing, and J.B. Goodenough: Double perovskites as anode materials for solid-oxide fuel cells. *Science* **312**, 254 (2006).
115. K.T. Lee, C.M. Gore, and E.D. Wachsman: Performance of lower temperature solid oxide fuel cells operating on reformed hydrocarbon fuels. *J. Power Sources* (2012, submitted).
116. K.T. Lee, D.W. Jung, H.S. Yoon, M. Camaratta, N. Sexson, and E. Wachsman: High performance LSM-ESB cathode on ESB electrolyte for low to intermediate temperature solid oxide fuel cells. *ECS Trans.* **35**, 1861 (2011).

https://doi.org/10.1557/jmr.2012.194 Published online by Cambridge University Press